Alternative signatures of the quintuplet fermions at the LHC and future linear colliders

Nilanjana Kumar [1,2,*] and Vandana Sahdev [1,†]

[1] *University of Delhi, New Delhi, India*

[2] *Centre for Cosmology and Science Popularization, SGT University, Gurugram, Delhi-NCR, India*

(Received 1 February 2022; accepted 20 May 2022; published 22 June 2022)

Large fermionic multiplets appear in different extensions of the Standard Model (SM), which are essential to predict small neutrino masses, relic abundance of the dark matter, and the measured value of muon anomalous magnetic moment [muon $(g-2)$]. Models containing a quintuplet of fermions (Σ), along with other scalar multiplets, can address recent anomalies in the flavor sector while satisfying the constraints from the electroweak physics. In standard scenarios, the exotic fermions couple with the SM particles directly and there exists a strong limit on their masses from collider experiments such as the Large Hadron Collider (LHC). In this paper, we choose a particular scenario where the quintuplet fermions are heavier than the scalars, which is naturally motivated from the muon $(g-2)$ data. A unique nature of these models is that they predict nonstandard signatures at the colliders as the quintuplet fermions decay via the scalars once produced at the colliders. We study these nonstandard interactions and provide alternative search strategies for these exotic fermions at the LHC and future linear colliders (such as e^+e^- colliders). We also discuss their exclusion and discovery limits. For the doubly charged quintuplet fermion ($\Sigma^{\pm\pm}$), discovery is possible with 5σ significance at integrated luminosity of 3000 fb^{-1} at the 14 TeV LHC if $M_\Sigma \leq 980$ GeV. For the singly charged quintuplet fermion ($\Sigma^\pm$), the discovery is challenging at the LHC but there might be a possibility of 5σ discovery with 1000 fb^{-1} luminosity at e^+e^- collider for $M_\Sigma \leq 700$ GeV.

DOI: 10.1103/PhysRevD.105.115016

I. INTRODUCTION

The Standard Model of particle physics has been observed with great precision at the experiments. The last missing piece, the Higgs boson, was discovered by ATLAS [1] and CMS [2] at the Large Hadron Collider (LHC) in 2012. However, it has some shortcomings—it is not possible to account for the small neutrino masses or the existence of dark matter in the SM, for instance. It is also difficult to explain the current measurement of muon $(g-2)$ [3] and the outcomes of flavor experiments [4] within the SM framework.

The small neutrino masses can be achieved by introducing exotic particles at a high scale via the effective dimension-five Weinberg operator at tree level *vis-à-vis* the seesaw mechanism. These extra particles correspond to a heavy fermion singlet, a scalar triplet, and a fermion triplet in type I, II, and III seesaw mechanisms, respectively [5–12]. However, there are other models, where the exotic particle content involves one or more larger multiplets of scalars and fermions together. These models [13–22] not only explain the small neutrino masses but also provide an explanation for the muon $(g-2)$ data, flavor anomalies while also predicting a suitable dark matter (DM) candidate in some cases. Such models also predict exotic signatures at the colliders.

A good example of such models are cascade seesawlike scenarios [13–16], where the neutrino mass is generated via a higher-dimensional $(5+4n)$ operator, where $n=1$ is the minimal scenario with three generations of Majorana quintuplets Σ_R, with hypercharge $Y=0$, and a scalar quadruplet Φ, with hypercharge $Y=-1$. Another example is the left-right symmetric framework [17,18] with an $SU(2)_R$ quintuplet where the gauge group is extended to $SU(3)_C \times SU(2)_L \times SU(2)_R \times U(1)_{B-L}$. In these models, the presence of a right-handed neutrino in the particle spectrum is essentially governed by the gauge structure and hence naturally explains the origin of light neutrino masses. Further, the neutral component of the quintuplet can be a DM candidate [19,20]. In models such as Radiative Neutrino Minimal Dark Matter model (RνMDM) [16,21], purely radiative neutrino masses are generated while also

*nilanjana.kumar@gmail.com
†vandanasahdev20@gmail.com

providing a viable DM candidate [22]. Models with both exotic fermions and charged scalars can also be motivated from the little Higgs scenarios [23], where the global symmetry is $SU(6)/Sp(6)$. These models successfully explain the flavor anomalies [24] and the signatures can be studied at the colliders. Additionally, doubly charged fermions (leptons) appear in weak isospin composite models as studied in Refs. [25–27]. Multicharged fermions also arise in other models including warped extra dimension models as shown in Refs. [28–35].

In this paper, we are motivated by a model with one quartet and one septet scalar field and quintuplet Majorana fermions (three copies) [36]. The interactions between the SM $SU(2)_L$ lepton doublets and these large multiplets induce neutrino masses which are suppressed by small vacuum expectation values (VEVs) of the quartet and/or the septet and also by the inverse of the quintuplet fermion mass (∼TeV). As a result, the scale of the neutrino Yukawa coupling can be reached to less than $\mathcal{O}(1)$ [36,37]. Further, this type of model is safe from any quantum anomaly, given the zero $U(1)_Y$ charge of these quintuplet fermions. There is no contribution to $SU(2)$ gauge anomaly as well.

The contents of the quintuplet are doubly charged fermions, singly charged fermions, and a neutral fermion [36]. Signatures of quintuplet fermions at the LHC have been studied in Refs. [38,39]. These fermions are also good candidates for exotic particle search in the future collider experiments [40,41]. In most of the phenomenological studies involving the quintuplet fermions, they decay directly into the SM particles. Even in scenarios as in Ref. [16], where interactions between the quintuplet fermions and the scalar multiplets are allowed, the fermions cannot decay into the scalars as the scalars are slightly heavier than the fermions. However, in our scenario [37], a small mass difference between the scalar multiplets and the fermionic quintuplet is naturally implied from muon $(g-2)$ and in such a way that the quintuplet fermions are heavier than the scalars.

In this paper, we study the signatures of the singly and doubly charged quintuplet fermions (Σ_R) at the hadron collider (pp collider) and linear colliders such as e^+e^- colliders, with each having its own advantages. Although the LHC has a much higher energy reach, the e^+e^- colliders provide a cleaner environment for distinguishing the signal from the background [42] and are more suitable for precision measurements [43]. With many e^+e^- colliders, such as FCC-ee, ILC, and CLIC in development stage, it would be interesting to study the discovery potential of the exotic quintuplet fermions at these colliders.[1]

Cases studied so far include multilepton and multijet signatures of the quintuplet fermions, both at the LHC [16,38] and the linear colliders [40,41,44]. As already stated, the quintuplet fermions in the scenario considered here decay into the SM particles via the scalars, which leads to final states containing a large number of leptons and jets. Such signals for quintuplet fermions have not been studied before. Given the many particle final states, it is difficult to reconstruct the masses of the fermion quintuplets or the scalars. However, we show that, by carefully choosing the final states from among the many possibilities, it is indeed possible to reconstruct both the masses. The masses of the exotic fermions, such as vectorlike quarks and leptons, are constrained to be more than ∼1 TeV [45,46] and ≥740 GeV [47], respectively. However, for this model, we choose to explore masses much below 1 TeV as well as masses larger than 1 TeV, considering the nonstandard decay modes of the quintuplet fermions.

For the singly charged scalar, the direct search limit from the large electron positron collider is 80 GeV [48]. However, the limit on the production cross section of the singly charged scalar as a function of its mass is given in Ref. [49]. Depending on the model under study, the charged scalars have fermiophobic or fermiophilic decay modes. Multilepton states where the doubly charged scalar decays into two same sign leptons are already studied in Refs. [33,50,51]. The lower mass limit ranges from about 230 to 870 GeV. On the other hand, if the doubly charged scalar decays to two same charge W bosons, the lower mass limit is placed between 200 and 350 GeV [51,52] in multilepton final states. However, in this paper we do not produce the charged scalars directly; they come as the decay product of the quintuplet fermions. Hence, in this analysis we have kept the lower limit on the scalar masses at 200 GeV and the mass of the scalars is chosen to be well below the mass of the quintuplet fermions ($\Delta M \sim 100$ GeV) to facilitate the decays of the quintuplet fermions via the scalars.

The rest of the paper is arranged as follows: The model is described in Sec. II. Collider signatures at the LHC and linear collider are described in Secs. III and IV, respectively. We discuss the results and conclude in Sec. V.

II. MODEL

We consider a simple scenario based on the models proposed in Refs. [36,37]. In the model of Ref. [36], the interaction among the SM $SU(2)_L$ lepton doublets and scalar multiplets, quartet (ϕ_4, $Y = 1/2$), and septet (ϕ_7, $Y = 1$) can induce neutrino masses, while preserving the ρ parameter. In order to achieve that, it is also necessary to introduce a quintuplet Majorana fermion Σ_R, with $Y = 0$. The neutrino masses are suppressed by the small VEVs of the quartet or septet and an inverse of the quintuplet fermion mass, which explains the smallness of the neutrino mass while also relaxing the Yukawa hierarchies. In order to make the generation of the neutrino mass more natural, an additional quintet scalar field (ϕ_5, $Y = 0$) with a nonzero VEV can be introduced [37]. As a result, tree-level neutrino mass is forbidden and the quartet scalar is an inert scalar,

[1]This model also offers interesting signatures for the charged scalars, which we do not address here.

while neutrino mass is generated at one-loop level. The model is further constrained from lepton flavor violation and the muon anomalous magnetic moment (Δa_μ).

In these models, the interesting point to note is that the quintuplet fermion Σ_R does not decay to Standard Model particles directly. Instead, it happens via its interaction with the charged scalars. Our objective is to study this particular scenario. Hence, we choose a simplistic scenario with quintuplet fermion Σ_R ($Y = 0$) and the quartet scalar ϕ_4 ($Y = 1/2$), along with their components[2]

$$\Phi_4 = (\varphi^{++}, \varphi_2^+, \varphi^0, \varphi_1^-)^T,$$
$$\Sigma_R = [\Sigma_1^{++}, \Sigma_1^+, \Sigma^0, \Sigma_2^+, \Sigma_2^{++}]_R^T, \tag{1}$$

where ($\Sigma_1^\pm$, $\Sigma_1^{\pm\pm}$) and ($\Sigma_2^\pm$, $\Sigma_2^{\pm\pm}$) are combined to make singly and doubly charged Dirac fermions, which we denote as $\Sigma^\pm$ and $\Sigma^{\pm\pm}$, respectively, while Σ_R^0 remains a neutral Majorana fermion. The masses of each component are given by M_Σ at the tree level where mixing between the SM leptons is negligibly small. The Yukawa interaction can be written as

$$-\mathcal{L}_Y = (y_\ell)_{ii}\bar{L}_{L_i}He_{R_i} + (y_\nu)_{ij}[\bar{L}_{L_i}\tilde{\Phi}_4\Sigma_{R_j}] + (M_R)_i[\bar{\Sigma}^c_{R_i}\Sigma_{R_i}] + \text{H.c.} \tag{2}$$

The components of the quintuplet fermion can decay into quartet scalars and SM leptons via the Yukawa interaction given by the second term of the above equation as

$$\begin{aligned}-\mathcal{L}_{yuk} \supset{}& (y_\nu)_{ij}[\bar{L}_{L_i}\tilde{\Phi}_4\Sigma_{R_j}] + \text{H.c.}\\ ={}& (y_\nu)_{ij}\left[\bar{\nu}_{L_i}\left(\frac{1}{\sqrt{2}}\Sigma^0_{R_j}\varphi^{0*} + \frac{\sqrt{3}}{2}\Sigma^+_{1R_j}\varphi_1^- + \frac{1}{2}\Sigma^+_{2R_j}\varphi_2^- + \Sigma^{++}_{1R_j}\varphi^{--}\right)\right.\\ &\left. + \bar{\ell}_{L_i}\left(\frac{1}{\sqrt{2}}\Sigma^0_{R_j}\varphi_1^- + \frac{1}{2}\Sigma^+_{1R_j}\varphi^{--} + \frac{\sqrt{3}}{2}\Sigma^-_{2R_j}\varphi^{0*} + \Sigma^{--}_{2R_j}\varphi_2^+\right)\right] + \text{H.c.}\end{aligned} \tag{3}$$

The coupling y_ν, as given in Eq. (3), can be constrained from observables such as ν mass, Δa_μ, and flavor observables. Following the benchmark points in [36,37], this coupling varies between 0.001 and 1, depending on the scalar particle content of the model. As we are studying a more general scenario, for the phenomenological purpose, we choose a very conservative limit of 0.1 for y_ν.

The components of the quintuplet can be produced via gauge interactions given by

$$\begin{aligned}\bar{\Sigma}_R\gamma^\mu iD_\mu\Sigma_R \supset{}& \bar{\Sigma}^{++}\gamma^\mu(2eA_\mu + 2gc_WZ_\mu)\Sigma^{++} + \bar{\Sigma}^+\gamma^\mu(eA_\mu + gc_WZ_\mu)\Sigma^+\\ &-\sqrt{2}g\bar{\Sigma}^{++}\gamma^\mu W_\mu^+\Sigma^+ - \sqrt{3}g\bar{\Sigma}^+\gamma^\mu W_\mu^+\Sigma_R^0 - \frac{\sqrt{5}g}{\sqrt{2}}\bar{\Sigma}^+\gamma^\mu W_\mu^+\Sigma_R^{0c}\\ &-\sqrt{2}g\bar{\Sigma}^+\gamma^\mu W_\mu^-\Sigma^{++} - \sqrt{3}g\bar{\Sigma}_R^0\gamma^\mu W_\mu^-\Sigma^+ - \frac{\sqrt{5}g}{\sqrt{2}}\bar{\Sigma}_R^{0c}\gamma^\mu W_\mu^-\Sigma^+,\end{aligned} \tag{4}$$

where $s_W(c_W) = \sin\theta_W(\cos\theta_W)$ with the Weinberg angle θ_W.[3]

The relevant gauge interactions associated with ϕ_4 can be obtained from the following kinetic term:

$$|D_\mu\Phi_4|^2 \supset \sqrt{\frac{3}{2}}v_4W^\pm W^\pm\varphi^{\mp\mp} + \frac{g^2v_4}{c_W}\left[s_W^2Z_\mu W^{+\mu}\varphi_2^- + \frac{\sqrt{3}}{2}(2 - s_W^2)Z_\mu W^{+\mu}\varphi_1^- + \text{c.c.}\right]. \tag{5}$$

Here, we have neglected the mixings among the individual components of the multiplets and we choose the components of the quintuplet fermion as well as scalar multiplets to be degenerate, which we denote as M_Σ and M_ϕ, respectively [36]. We also consider $M_\Sigma > M_\phi$, which is naturally implied from the muon anomalous magnetic moment measurement, as shown in [37]. For the complete Lagrangian, we refer to Ref. [36].

Further, considering the interactions in Eq. (3), $\Sigma^\pm$ and $\Sigma^{\pm\pm}$ can decay via the following modes:

$$\Sigma^\pm \to \phi_2^\pm(\phi_1^\pm)\nu(\bar{\nu}),$$
$$\Sigma^\pm \to \phi^{\pm\pm}l^\mp,$$
$$\Sigma^\pm \to \phi^0l^\pm, \tag{6}$$

[2]Even in the models with more than one scalar multiplet, the components mix during mass diagonalization and charged and neutral scalar mass eigenstates are obtained.

[3]The components of ϕ_4 can also be produced at the collider via the gauge interaction, as shown in Ref. [36].

$$\Sigma^{\pm\pm} \to \phi^{\pm\pm}\nu(\bar{\nu}),$$
$$\Sigma^{\pm\pm} \to \phi_2^{\pm} l^{\pm}. \quad (7)$$

The branching ratios are assumed to be the same in each decay mode of $\Sigma^{\pm}$ and $\Sigma^{\pm\pm}$. Interactions in Eq. (5) allow the decays of the charged scalars into SM gauge bosons *viz*,

$$\phi_2^{\pm}(\phi_1^{\pm}) \to W^{\pm}Z,$$
$$\phi^{\pm\pm} \to W^{\pm}W^{\pm},$$
$$\phi^{0} \to W^{+}W^{-}. \quad (8)$$

In the following sections, we perform a collider study of the $\Sigma^{\pm}$ and $\Sigma^{\pm\pm}$ when they decay via the scalars.[4] Even though there are many possible production modes, [38], we study the pair production of $\Sigma^{\pm}$ and $\Sigma^{\pm\pm}$. This is because it will be easier to reconstruct the masses of the quintuplets if they are produced in pairs. As can be seen from the decay modes, the final states will have a rich collection of leptons and jets. The phenomenology of these alternative signatures is what we study next.

III. PHENOMENOLOGY AT THE *pp* COLLIDER

In this section, we discuss the collider physics of the quintuplet fermions at the LHC. They can be produced in pp collisions through s- and t-channel processes via Z/γ and $\Sigma^{\pm}$ (or $\Sigma^{\pm\pm}$), respectively. The cross sections for the production of the singly charged fermions $pp \to \Sigma^{+}\Sigma^{-}$ are smaller in comparison to those for the doubly charged fermions $pp \to \Sigma^{++}\Sigma^{--}$, as shown in Ref. [36]. Moreover, we have also considered the photon-photon fusion in the pp collision; the matrix element squared for pair production of the exotic fermions is enhanced by a factor of $(Q)^4$, where Q is the charge of the fermion. Even then, the cross section for the singly charged fermions was not sufficient to produce a significant signal-to-background ratio. Hence, we choose to study only the pair production of doubly charged fermions at the LHC, for which we show the Feynman diagrams in Fig. 1. In Fig. 2, we have shown the cross section for the pair production $pp \to \Sigma^{++}\Sigma^{--}$ at different values of $\sqrt{s}$ at the LHC, where $p = q, \bar{q}, \gamma$. For comparison, the cross section for $pp \to \Sigma^{+}\Sigma^{-}$ is also shown at $\sqrt{s} = 14$ TeV by the dotted curve in blue.

The inclusion of the photon parton distribution function (PDF) increases the signal cross section significantly. Moreover, inclusion of photon PDF is important for the consistency of the calculation as the other PDFs are determined up to next-to-next-leading order in QCD. We would like to note that, in view of the above, Neural Network PDF (NNPDF) [53,54], Martin-Roberts-Sterling-Thorne PDF (MRST) [55], and Coordinated Theoretical/Experimental project on QCD phenomenology and tests of the standard model (CTEQ) [56] already include photon PDFs in their definitions. In order to compute the cross sections and generate events at the LHC, we incorporate the model Lagrangian in FeynRules (v2.3.13) [57,58]. Using FeynRules, we generate the model file for MadGraph5_aMC@NLO (v2.2.1) [59]. For the cross sections, we use the NNPDF23LO1 parton distributions [60] with the factorization and renormalization scales at the central m_T^2 scale after k_T clustering of the event.

[4] Hereafter, we use the notation $\phi^{\pm}$ for $\phi_1^{\pm}$ and $\phi_2^{\pm}$.

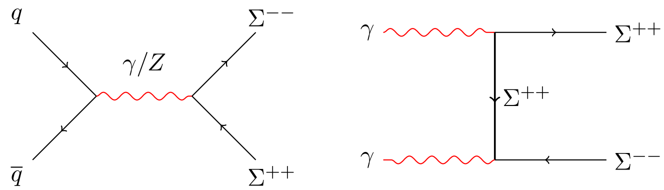

FIG. 1. Feynman diagrams for the production of doubly charged fermions ($\Sigma^{\pm\pm}$) at pp collider.

A. Signal

Once pair produced at the LHC, the decays of the doubly charged fermions produce the following states:

$$\Sigma^{++} \to \phi^{++}\nu \to (W^{+}W^{+})\nu; \quad \Sigma^{--} \to \phi^{--}\bar{\nu} \to (W^{-}W^{-})\bar{\nu},$$
$$\Sigma^{++} \to \phi^{++}\nu \to (W^{+}W^{+})\nu; \quad \Sigma^{--} \to \phi^{-}l^{-} \to (W^{-}Z)l^{-},$$
$$\Sigma^{++} \to \phi^{+}l^{+} \to (W^{+}Z)l^{+}; \quad \Sigma^{--} \to \phi^{-}l^{-} \to (W^{-}Z)l^{-}, \quad (9)$$

with conjugate processes included in each case. The branching ratio in each case is assumed to be the same, as discussed in the previous section. This gives rise to final states comprising a number of leptons, jets, and missing energy, resulting in various multilepton, multijet, and mixed states. After carefully analyzing each of them on the basis of performance over SM backgrounds and mass reconstruction of the doubly charged fermions, we decide upon two channels:

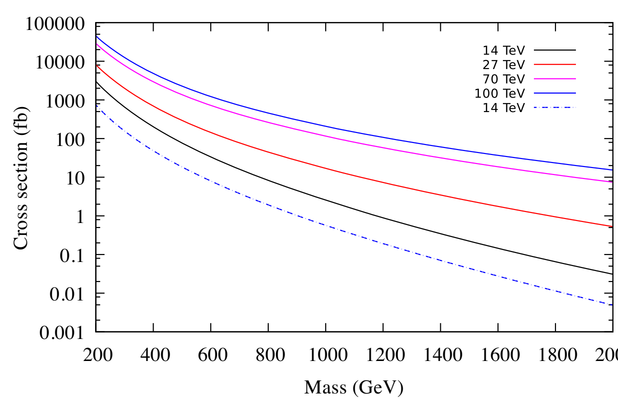

FIG. 2. Signal cross section for the process $pp \to \Sigma^{++}\Sigma^{--}$, where $p = q, \bar{q}, \gamma$ as a function of M_{Σ} at different $\sqrt{s}$ is shown by the solid lines. The dotted line represents the process $pp \to \Sigma^{+}\Sigma^{-}$ at 14 TeV.

TABLE I. Selections $S1$, $S2$, and $S3$ for channels I and II.

Selections	Channel I	Channel II
$S0$	$N(\ell) \geq 4$	$N(\ell) \geq 3 + N(j) \geq 2$
$S1$	$p_T(l) > 30$ GeV $\lvert\eta\rvert(l) < 2.5$ $\Delta R_{\ell\ell/j} > 0.3$	$p_T(l) > 30$ GeV $\lvert\eta\rvert(l) < 2.5$ $\Delta R_{\ell\ell/j} > 0.3$ $p_T(j) > 30$ GeV $\lvert\eta\rvert(j) < 2.5$ $\Delta R_{jj} > 0.3$
$S2$	$S_T(l) > 400$ GeV $M(\ell^+, \ell^+), M(\ell^-, \ell^-) > 100$ GeV $\Delta R(\ell_0, \ell_1) > 1.5$	$S_T(l) > 200$ GeV $M(\ell^\pm, \ell^\pm) > 100$ GeV $\Delta R(\ell, \ell) > 1.5$ $H_T(j) > 300$ GeV
$S3$		60 GeV $< M(j, j) <$ 120 GeV $(M_\phi - 100) < M(j, j, \ell) < (M_\phi + 100)$

(i) Channel I: $\geq 4\ell$ channel with two pairs of same sign (SS) leptons $(l^+l^+), (l^-l^-) +$ MET, where both the pairs are oppositely charged.

(ii) Channel II: $\geq 3\ell + 2$ jets channel with at least one pair of SS leptons $(l^\pm l^\pm)$+one isolated lepton $(l^\mp) +$ MET.

Here, $\ell = e, \mu, \tau$. We also check the efficiency for the channel $4\ell + 1/2$ jets, but the efficiency turns out to be less compared to channels I and II. For the $4\ell + 3/4$ jets channel, the signal and background cross sections both are significantly low. Even though it is possible to obtain a better significance in this channel, the number of signal events to be observed at 3000 fb^{-1} integrated luminosity is less than 10. Hence, we do not pursue this channel. Also, in a purely leptonic channel, the leptons in the final states are either coming from the decay of $\Sigma^{\pm\pm}$ or from W/Z. Hence, the transverse mass of the leptons can be reconstructed, but clear mass reconstruction of the quintuplet mass is difficult as there are different sources of MET. However, the $\geq 4\ell$ channel with the additional criteria, as in channel I, predicts a good S/B ratio, and hence we study it. The requirement of at least four leptons as well as the two SS lepton pairs in channel I makes it much cleaner compared to other channels, even though we do not put any restriction on the number of jets. We do not impose any jet or b-jet veto in channel I as this will result in a lesser number of signal events. Also, we do not go beyond the four-lepton requirement because the signal cross section $\times$ branching ratio (BR) falls off due to a smaller branching ratio of W and Z into leptons. In channel II, we include both leptons and jets in the final states and we show that a clear mass reconstruction of $\phi^\pm$ or $\phi^{\pm\pm}$[5] and $\Sigma^{\pm\pm}$ is possible.

We choose five benchmark points (BPs) in our study *viz* BP1 ($M_\phi = 200$, $M_\Sigma = 300$ TeV), BP2 ($M_\phi = 500$ TeV, $M_\Sigma = 600$ TeV), BP3 ($M_\phi = 700$ TeV, $M_\Sigma = 800$ TeV), BP4 ($M_\phi = 900$ TeV, $M_\Sigma = 1000$ TeV), BP5 ($M_\phi = 1000$ TeV, $M_\Sigma = 1200$ TeV). We do not study the signal for M_Σ larger than 1.2 TeV due to two reasons. First, the cross section is small at a larger mass of Σ. Second, when $M_\Sigma > 1.2$ TeV, the decay products of W and Z bosons become collimated and the probability of observing them as a fat jet is larger and the analysis process will be very different. The fat jet scenario will also be ideal for 27 TeV c.m. energy.

B. Backgrounds

The main backgrounds for channels I and II come from inclusive diboson production, $VV +$ jets, where $V = W, Z$. There will also be contributions from triboson ($VVV +$ jets), $HV +$ jets, and $t\bar{t}V +$ jets. The contributions from the $t\bar{t}VV +$ jets and four-top backgrounds are found to be negligible. For channel II, additionally, we get comparatively less contribution from $t\bar{t} +$ jets and $V +$ jets and for channel I, they are negligible. In [61] and the references therein, the cross section of these channels has been discussed in detail.

C. Collider analysis

As a potential signature, we prefer the SS lepton pairs over the opposite sign (OS) leptons, due to the abundance of the former in the signal. This is because of the decay of the quintuplets via the charged scalars, as shown earlier. On the other hand, the SM backgrounds involving one or more than one Z, are more likely to involve an OS pair of leptons. Hence the signatures involving the SS pair of leptons suffer from less SM background. The signal and background are optimized over a set of selections, which we list in Table I.

1. Channel I: $\geq 4\ell$ channel with (l^+l^+) and (l^-l^-) pair + MET

In the multilepton searches performed for exotic particles (vector like leptons, charged scalars, etc.), only one OS or

[5] As they have the same mass.

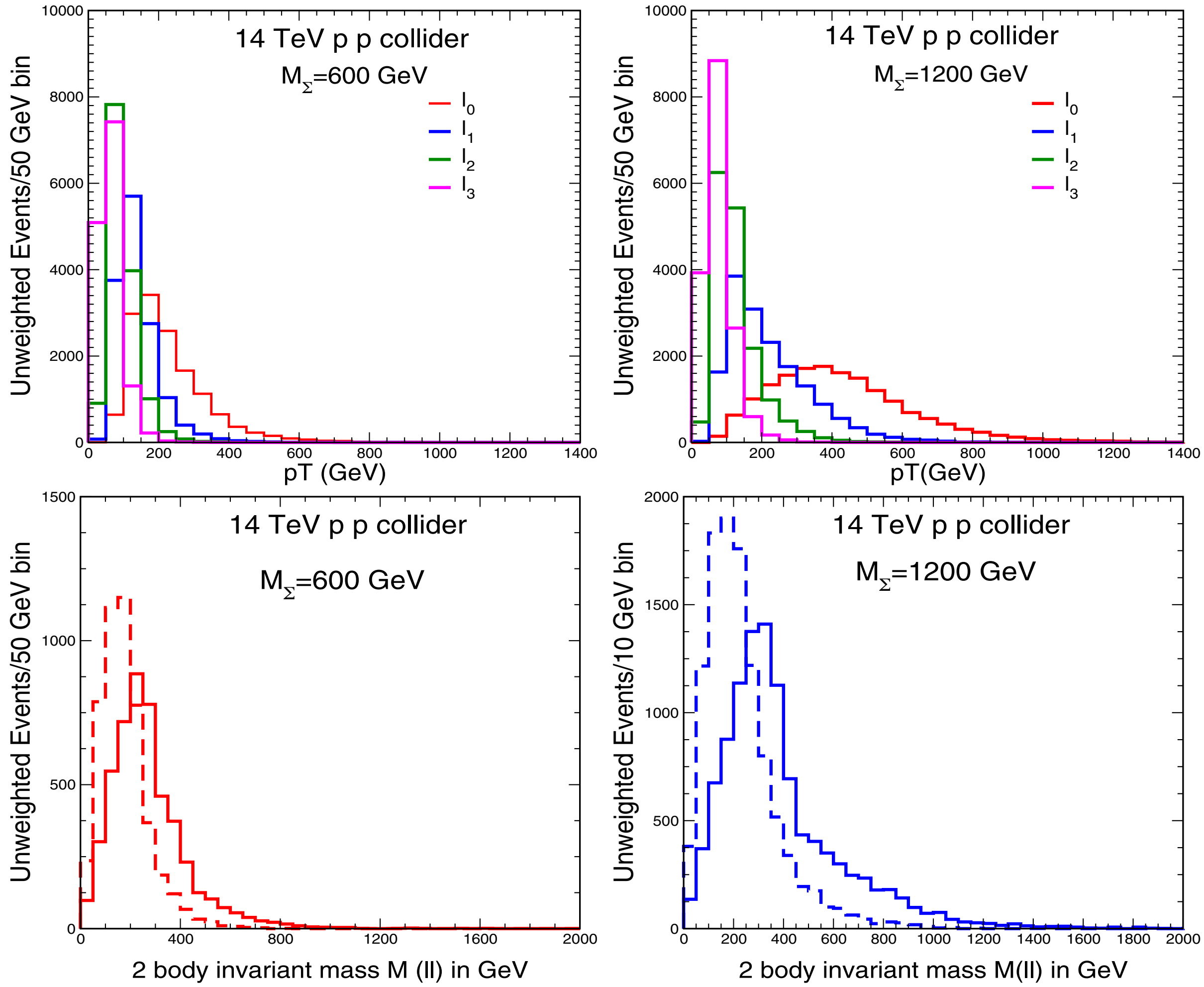

FIG. 3. Top: distributions of $pT(l)$ and (bottom) same sign lepton pair invariant mass distributions for $M_\Sigma = 600$ and 1200 GeV (BP2 and BP5), respectively, in channel I at the 14 TeV LHC. The solid and dashed lines correspond to the first and second pairs of SS leptons.

SS pair is identified in most of the cases, the only exception being the searches for multicharged scalars [50]. This is largely due to the standard decay modes of the beyond the SM particles. On the other hand, in channel I, we have the requirement of two SS lepton pairs, with pairwise opposite charges. In channel I, the quintuplet fermions decay to Z and/or W via the charged scalars, and most of the final state leptons come from the decay of the Z/W bosons. Hence, we do not apply any Z/W veto. We arrange the leptons (ℓ_i) in the descending order of pT. In this channel, the SS leptons appear directly from the direct decay of $\Sigma^{\pm\pm}$ and from the decay of W/Z decay in the same decay chain. We plot the lepton's pT and the invariant mass distribution of the SS lepton pairs for two BPs (BP2 and BP5) in Fig. 3. The solid line represents the invariant mass distribution if at least one SS pair is present, and the dotted line represents the same for the additional SS pair, where these two pairs have opposite charge. Based on the two-body mass distribution, we have imposed the selection $M(\ell^\pm, \ell^\pm) > 100$GeV.

In Fig. 4, we plot the sum of lepton pT [$S_T(\ell)$] and missing transverse energy (MET) distributions for the signal and the total background. Note that a substantial amount of MET is present in the signal, as well as in the SM background. Hence, we refrain from putting any cut on MET in order to get most of the signal events. Even though the signal has a very high $S_T(\ell)$ compared to the background, the set of selections optimize for $S_T(\ell) >$ 400 GeV for the whole signal region under consideration. For example, if we focus on the region $M_\Sigma > 1$ TeV only, $S_T(\ell) > 600$ GeV gives a much better S/B ratio. However, we choose to use only one value for the $S_T(\ell)$ selection for our BPs. Based on the plots of the kinematic variables, we optimize the selections at the given values in Table I. We find that the cut on $S_T(\ell)$ is sufficient to suppress the background in channel I. Moreover, the leptons with the highest pT will have a larger separation compared to the other leptons, as they are from the separate decay chains of the quintuplet, in most of the cases. Thus, we impose a selection on these leptons by requiring $\Delta R(\ell_0, \ell_1) > 1.5$.

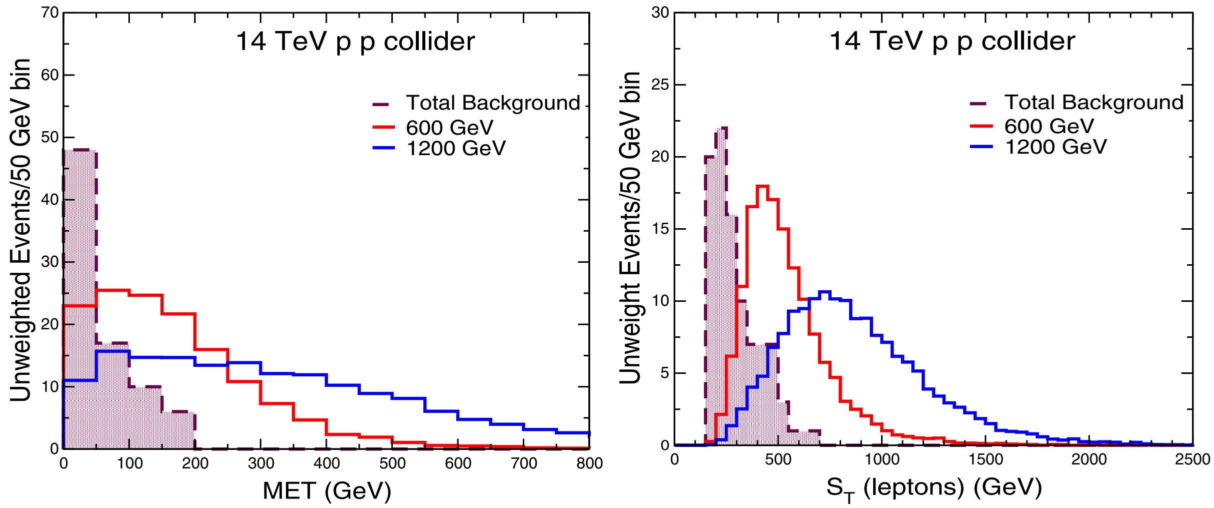

FIG. 4. Left: transverse missing energy and (right) sum of lepton pT $[S_T(\ell)]$ distribution for $M_\Sigma = 600$ and 1200 GeV and total background (shadowed region) in channel I.

In Tables II and III, we summarize the effect of the selections in channel I with (l^+l^+) and (l^-l^-) pair + MET. As there is no jet veto imposed, the majority of the backgrounds come from the diboson + jets events. Initially, this background cross section is comparably very high but after we impose the selection S_2, the background reduces further.

2. Channel II: $\geq 3\ell$ channel with $(l^\pm l^\pm)$ pair + $l^\mp$ + ≥ 2 jets channel

In this channel, we require the presence of at least three leptons as well as two or more jets. In Fig. 5, we show the p_T distributions of the jets and also the sum of pT for the jets $[H_T(j)]$. The pT distribution of the leptons is mostly the same as channel I, but as the number of leptons in channel II is less than channel I, the $S_T(\ell)$ distribution peaks at a lower value compared to channel I. In channel II, we identify at least one SS lepton pair in a manner as stated in channel I. The selections in channel II are summarized in Table I. Additionally, we find that a cut on the minimum value of $H_T(j)$ is useful to minimize the background.

TABLE II. The variation of the cross section (femtobarn) for each of the BPs, as the selections are imposed at the 14 TeV LHC in channel I.

M_Σ (GeV)	$S1$ (fb)	$S2$ (fb)
BP1, 300	2.335	1.093
BP2, 600	0.598	0.219
BP3, 800	0.196	0.093
BP4, 1000	0.063	0.032
BP5, 1200	0.024	0.013

TABLE III. Same variation as Table II for the background.

Major backgrounds	$S1$ (fb)	$S2$ (fb)
Diboson + jets	20.42	0.55
$t\bar{t}V$	0.25	0.07
Triboson	0.082	0.022
HV + jets	0.048	0.021
Total	20.80	0.66

The main objectives in channel II are to construct the three- and four-body invariant mass distributions, $M(\ell jj)$ and $M(\ell\ell jj)$, for the reconstruction of M_ϕ and M_Σ, respectively. Note that this is only possible when we consider the decay of the quintuplet via the singly charged scalar. Even though it is theoretically possible to reconstruct the mass of the quintuplet from $M(\ell jjj)$ also, it is harder to select the exact jets for the distribution. Hence, we consider the case when W and Z decay through leptonic and hadronic modes, respectively. At first, we select two SS leptons in such a way that they must come from the same decay chain. One lepton is coming from the decay of the quintuplet and the another is from the W. We demand $\Delta R(\ell\ell) > 1.5$ for these two leptons. Then, we select two jets coming from the decay of the Z boson, by requiring $60 < M(jj) < 120$ GeV. The three-body mass distribution $M(\ell jj)$ and the four-body mass distribution $M(\ell\ell jj)$ reconstruct the masses of ϕ and $\Sigma^\pm$, which is shown in Fig. 6. We select the final events with S_3, where the events are required to satisfy the three-body invariant mass in the window of $M_\phi \pm 100$ GeV. The signal and background cross section after the cuts are shown in Tables IV and V. Clearly, the selection after S_3 gives a better signal-to-background ratio.

3. Result

The significance for the discovery can be described as (see Refs. [62–64])

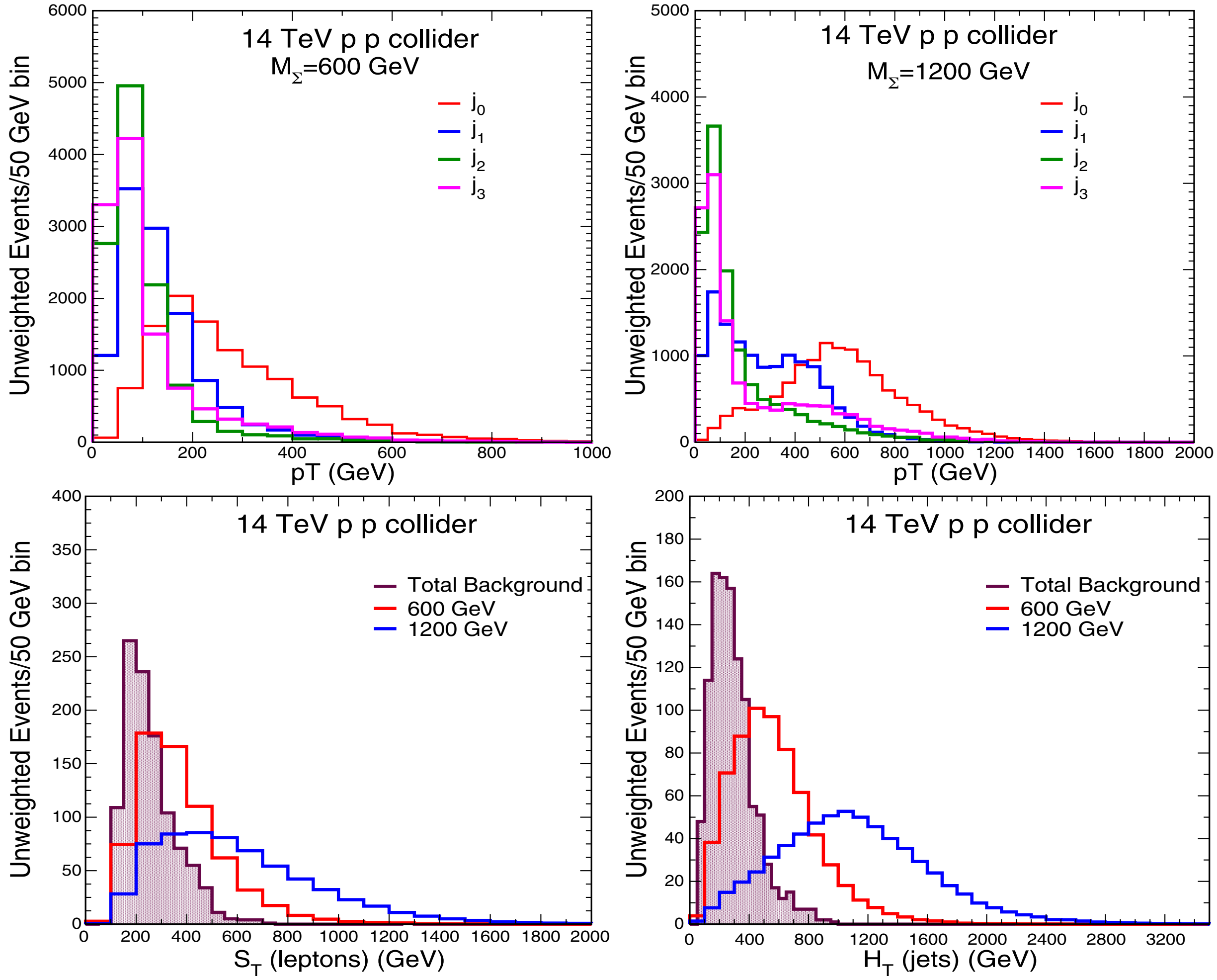

FIG. 5. Top: distributions of jet pT and (bottom) sum of lepton pT $[S_T(\ell)]$ (left) and sum of jet pT $[H_T(j)]$ (right), for $M_\Sigma = 600$ and 1200 GeV, respectively, for channel II at the 14 TeV LHC. The shadowed region corresponds to the total background.

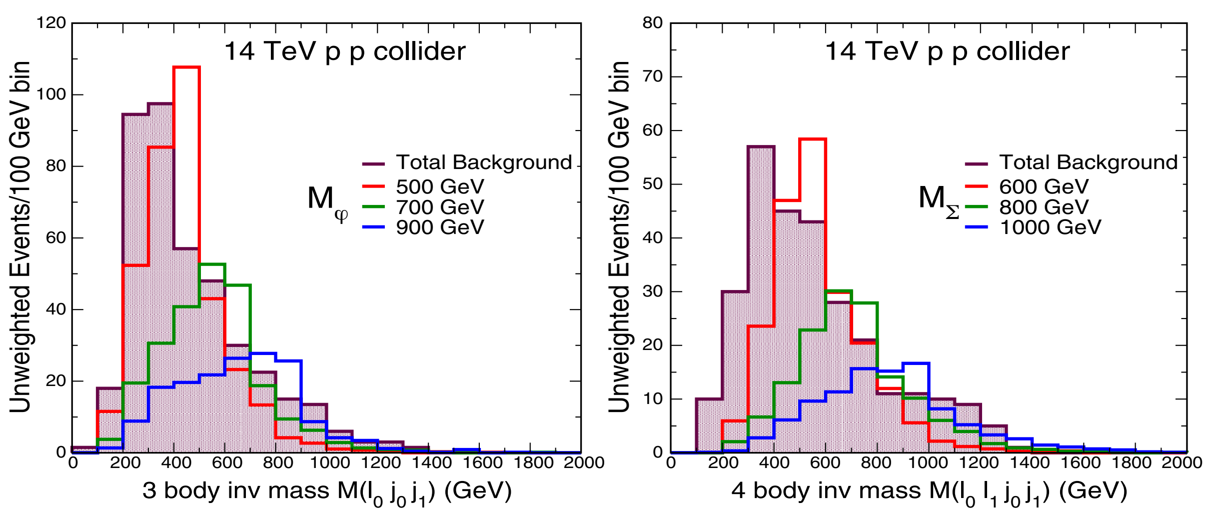

FIG. 6. Left: three-body invariant mass $M(\ell jj)$ and (right) four-body invariant mass $M(\ell\ell jj)$ for $M_\phi = 500$, 700, 900 GeV and $M_\Sigma = 600$, 800, 1000 GeV, respectively, for channel II at the 14 TeV LHC. The shadowed region corresponds to the total background.

TABLE IV. The variation of the signal cross section (femtobarn) for each of the BPs, as the selections are imposed at the 14 TeV LHC.

M_Σ (GeV)	$S1$	$S2$	$S3$
BP1, 300	11.55	4.4	0.112
BP2, 600	2.85	1.025	0.028
BP3, 800	0.84	0.39	0.007
BP4, 1000	0.25	0.14	0.0017
BP5, 1200	0.09	0.054	0.0005

$$Z_{\rm dis} = \left[2\left((s+b)\ln\left[\frac{(s+b)(b+\Delta_b^2)}{b^2+(s+b)\Delta_b^2}\right] - \frac{b^2}{\Delta_b^2}\ln\left[1+\frac{\Delta_b^2 s}{b(b+\Delta_b^2)}\right]\right)\right]^{1/2}, \tag{10}$$

where s and b are the number of signal and background events, respectively, and Δ_b is the uncertainty in the measurement of the background. If $\Delta_b = 0$,

$$Z_{\rm dis} = \sqrt{2[(s+b)\ln(1+s/b) - s]}.$$

If b is large,

$$Z_{\rm dis} = s/\sqrt{b}.$$

Thus, if b is small, $s/\sqrt{b}$ overestimates the significance. We use $Z_{\rm dis} > 5$ which corresponding to $p < 2.86 \times 10^{-7}$ for different values of Δ_b. Similarly, the significance for exclusion is

$$Z_{\rm exc} = \left[2\left\{s - b\ln\left(\frac{b+s+x}{2b}\right) - \frac{b^2}{\Delta_b^2}\ln\left(\frac{b-s+x}{2b}\right)\right\} - (b+s-x)(1+b/\Delta_b^2)\right]^{1/2}$$
$$x = \sqrt{(s+b)^2 - 4sb\Delta_b^2/(b+\Delta_b^2)}. \tag{11}$$

If $\Delta_b = 0$,

$$Z_{\rm exc} = \sqrt{2(s - b\ln(1+s/b))}.$$

For 95% C.L. exclusion ($p = 0.05$), we use $Z_{\rm exc} > 1.645$ for different Δ_b.

We calculate the significance using the formula in Eq. (10) in order to account for the uncertainty in the background, as the background is small in both the channels. The integrated luminosity for discovery and exclusion as a function of the mass of the doubly charged fermion (M_Σ) is shown in Fig. 7. The prediction in channel I is sensitive to the uncertainty in the background, which we have considered to be $\sigma_B = 0, 0.25 \times b, 0.5 \times b$. Channel II is not sensitive to σ_B as the signal and background cross sections both are small, as given in Tables IV and V. We have found that channels I and II have a good discovery potential for masses up to 850 and 1025 GeV, respectively, at 3000 fb^{-1} luminosity with $\sigma_B = 0$. In channel I, more than 3000 fb^{-1} luminosity is required for discovery of $M_\Sigma > 850$ GeV with nonzero σ_B.

Masses up to 1.05 and 1.2 TeV can be excluded with 95% C.L. (corresponds to Z value $= 1.645$) at 3000 fb^{-1} luminosity, with no background uncertainty. In channel I, with integrated luminosity of 3000 fb^{-1}, the exclusion limit is 1 TeV and 920 GeV for $\sigma_B = 0.25$ and 0.5, respectively. Hence, we find that channels I and II have a good prospect for both exclusion and discovery of the doubly charged fermions in the high luminosity (HL)-LHC, with 3000 fb^{-1}, with the added advantage of mass reconstruction for the doubly charged fermion and the charged scalar in channel II.

IV. PHENOMENOLOGY AT THE e^+e^- COLLIDER

We have shown in Sec. III that the pair production cross sections of the singly charged fermions ($\Sigma^\pm$) are smaller compared to the doubly charged fermions ($\Sigma^{\pm\pm}$) at pp collision, where both are components of a fermionic quintuplet. The small cross section makes it difficult to observe singly charged fermions at the 14 TeV LHC when we look for the alternative signatures in our model. Even increasing the center of mass energy further up to 27 TeV does not solve the issue. These singly and doubly charged fermions can also be produced in linear colliders, such as the e^+e^- collider, which in turn generate multiple leptons and jets in the final state. Even though it is possible to observe alternative signatures for both singly and doubly charged fermions at the e^+e^- colliders, we restrict ourself to the case of the singly charged fermion. The production of

TABLE V. Same variation as Table IV for the background.

Major backgrounds	$S1$	$S2$	$S3$ (BP1)	$S3$ (BP2)	$S3$ (BP3)	$S3$ (BP4)	$S3$ (BP5)
Diboson + jets	45.05	14.00	0.085	5.5×10^{-3}	3×10^{-4}	6×10^{-5}	1×10^{-5}
$t\bar{t}V$	10.42	0.53	0.056	1×10^{-3}	2×10^{-4}	2×10^{-5}	$<10^{-5}$
Triboson	0.336	0.013	0.004	$<10^{-3}$	$<10^{-4}$	$<10^{-5}$	$<10^{-6}$
HV + jets	1.2	0.012	0.003	$<10^{-3}$	$<10^{-4}$	$<10^{-5}$	$<10^{-6}$
Total	61.06	14.57	0.148	0.0065	0.0005	7×10^{-5}	1×10^{-5}

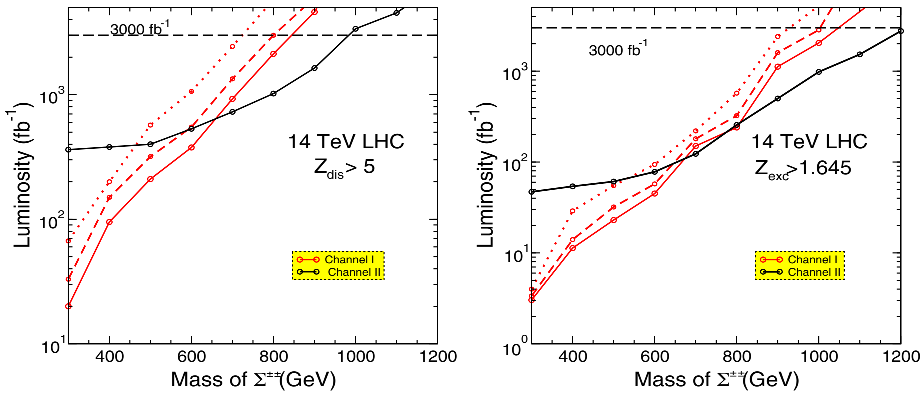

FIG. 7. The integrated luminosity for discovery (left) and exclusion (right) as a function of the mass of the doubly charged fermion at the 14 TeV LHC. The solid, dashed, and dotted lines correspond to 0%, 25%, and 50% uncertainty in the total background, respectively.

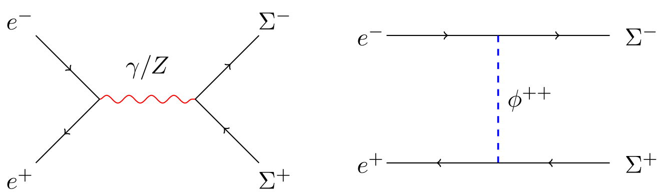

FIG. 8. Feynman diagrams for the production of singly charged quintuplet fermion at the e^+e^- collider.

the doubly charged fermions lead to more leptons and jets in the final state than the singly charged fermions. Here, we choose to study the final states once the singly charged fermions are produced in pair at e^+e^- collider. The analysis for the doubly charged fermions will be similar to this. Moreover, at the LHC, being a pp collider, the multijet signals are complicated to study due to the heavy QCD backgrounds. However, the e^+e^- collider offers a much cleaner environment. Hence, the SM background for the signal involving multiple jets are remarkably small compared to pp colliders.

A. Signal

The singly charged fermions ($\Sigma^{\pm}$) can be produced in pairs at the e^+e^- collider via the gauge couplings, as described in the previous section. The Feynman diagrams for the pair production are shown in Fig. 8. In general, the process proceeds through the s channel via γ and Z boson exchange. However, in this particular model, there is an extra contribution coming from the t-channel diagram via the doubly charged scalar. The cross section due to the t-channel diagram is large compared to the other diagram. However, the contribution in the total cross section is not so large, due to destructive interference between the s- and t-channel diagrams. The effect of the polarization of the electron and positron beam has been discussed in detail in Ref. [65], and we have followed the exact same polarization of the e^+ and e^- beam, which leads to maximum left-right asymmetry of -0.6 (A_{LR}).

The production cross sections are computed in MadGraph5_aMC@NLO (v2.6.5) with the normalization and factorization scales set at m_Z and shown in Fig. 9. For further study, we choose the following benchmark points: $M_\Sigma = 200$ GeV at $\sqrt{s} = 500$ GeV, $M_\Sigma = 300$ and 400 GeV at $\sqrt{s} = 1000$ GeV, and $M_\Sigma = 500$, 600, and 700 GeV for $\sqrt{s} = 1500$ GeV.[6]

The decays of the singly charged fermions lead to the following final states involving W/Z bosons,

governed by the equations in Sec. II. Among all the final states, the leptonic final states or final states of leptons + jets suffer from lower effective cross section due to the small branching ratio of W/Z into leptons. The signals with multiple jets have the advantage over multilepton states, as the branching ratio of W/Z is more into jets than leptons. The final states involving multiple jets can have a maximum of six jets, coming from the decays of W/Z. Here, we show a detailed analysis of two final states:

(i) Channel A: One lepton ($\ell^{\pm}$) + 4 jets.

(ii) Channel B: Two opposite sign lepton pair ($\ell^+\ell^-$) + 4 jets.

These types of signals in the e^+e^- collider have a greater chance for discovery due to a smaller background, which is also shown in [68].

B. Backgrounds

The major backgrounds for the channels under study get contributions from diboson (WW, ZZ), $t\bar{t}$, $t\bar{V}$, triboson ($VVV = ZZZ$, ZWW), and HZ production. The variation of these major backgrounds with $\sqrt{s}$ is already shown in [66]. Along with multileptons, as the channels under investigation include multiple jets, we demand *inclusive* cross section of these backgrounds by producing at least two jets in association, such as diboson + 2 jets production

[6]We did not go to masses beyond 700 GeV because it would require a 3 TeV linear collider. At large energies, the analysis will require a detailed study of fat jets (W/Z) [66,67], which emerge as decay products of the charged fermions.

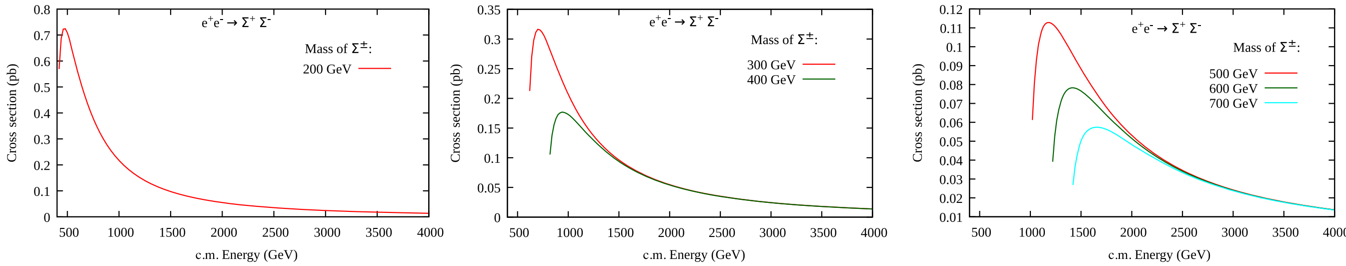

FIG. 9. Pair production cross sections for the singly charged fermions of different masses as a function of center of mass energy, at the e^+e^- collider.

TABLE VI. Selections $A1$ and $A2$ for channel A and channel B.

Selections	Channel A	Channel B
$A0$	$N(\ell) \geq 1 + N(j) \geq 4$	$N(\ell) \geq 2 + N(j) \geq 4$
$A1$	$p_T(l) > 10$ GeV $\lvert\eta\rvert(l) < 2.5$ $\Delta R(\ell, \ell/j) > 0.4$ $p_T(j) > 20$ GeV $\lvert\eta\rvert(j) < 5.0$ $\Delta R_{jj} > 0.4$	$p_T(l) > 10$ GeV $\lvert\eta\rvert(l) < 2.5$ $\Delta R(\ell, \ell) > 0.4$ $p_T(j) > 20$ GeV $\lvert\eta\rvert(j) < 5.0$ $\Delta R_{jj} > 0.4$
$A2$	$\Delta R(\ell, j) > 1.5$ $\cdots$	$\Delta R(\ell, j) > 1.5$ $M(\ell^+, \ell^-) > 100$ GeV

TABLE VII. Cross sections for the signal $e^+e^- \to \Sigma^+\Sigma^-$ before and after the selections. Channel (A) corresponds to $l^\pm + 4$ jets and channel B corresponds to $l^\pm l^\pm + 4$ jets.

$\sqrt{s}$	M_Σ (GeV)	σ (pb)	σ^A_{A2} (fb)	σ^B_{A2} (fb)
500 GeV	200	0.706	4.45	0.049
	200	0.218	15.70	0.131
1 TeV	300	0.209	14.63	0.125
	400	0.175	13.50	0.122
	500	0.089	7.56	0.107
1.5 TeV	600	0.077	7.24	0.1001
	700	0.05	4.95	0.09

($VVjj$), $t\bar{t} + 2$ jets, and $HZ + 2$ jets. The contribution from the $\ell\ell + 2$ jets, four jets, and four-top production are found to be small. We include these backgrounds in the "others" category. Among all the backgrounds, the cross section of $ZZjj$ is found to be larger.

C. Collider analysis

In order to generate events, we use MadGraph5_aMC@NLO (v2.2.1) [59], where the showering and hadronization are done in a similar way as mentioned before in the LHC part. In FastJet, the jets are reconstructed with distance parameter $R = 0.4$ using anti-K_t algorithm. In DELPHES, we use the DELPHES ILD card [69] for detector simulation. The signal and background events are required to pass through selections on different kinematic distributions, as given in Table VI. At first, we select events with basic cuts, $A1$. Later, while selecting the single lepton or the oppositely charged lepton pair, we make sure that it is well isolated from the jets coming from the decays of W/Z by requiring a moderate isolation cut in $A2$. We have also imposed a cut on $M(\ell^+, \ell^-)$ in channel B to reduce the background further.

The signal and background cross sections after the cuts are shown in Tables VII and VIII, respectively. We found the background to be small enough to give a very good signal-to-background ratio (S/B), after the initial cuts $A1$ for channel A. For channel B, in order to improve the S/B ratio, we have imposed further cuts in $A2$ on selected opposite sign lepton pairs ($\ell^+\ell^-$), as shown in Table VI.

TABLE VIII. Cross sections for various backgrounds corresponding to channels A ($l^\pm + 4$ jets) and B ($l^\pm l^\pm + 4$ jets) after the selections.

	σ^A_{A2} (fb)			σ^B_{A2} (fb)		
Background	$\sqrt{s} = 500$ GeV	1 TeV	1.5 TeV	$\sqrt{s} = 500$ GeV	1 TeV	1.5 TeV
Diboson + jets	8.08	3.04	1.63	0.0	0.0	0.0
$t\bar{t}$ + jets	82.5	24.75	11.25	1.1	0.33	0.15
$t\bar{t}V$	1.121	1.79	1.083	0.039	0.0614	0.037
VVV	2.85	5.0	3.67	0.0024	0.0035	0.0031
HV + jets	2.85	0.65	0.3	0.045	0.0	0.0
Others	$\cdots$	$\cdots$	$\cdots$	0.045	0.0425	0.035
Total	97.4	34.35	17.94	1.186	0.437	0.225

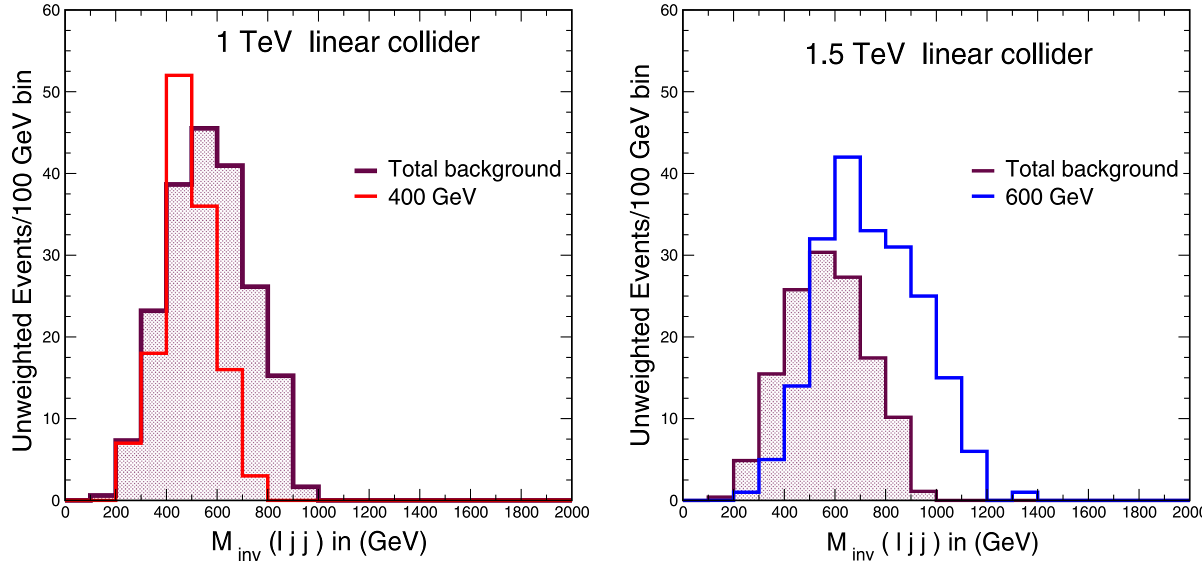

FIG. 10. Three-body invariant mass $M(\ell jj)$ for $M_\Sigma = 400$ GeV (left) and $M_\Sigma = 600$ GeV (right) for channel B at 1 and 1.5 TeV e^+e^- colliders, respectively. The shadowed region represents the total background.

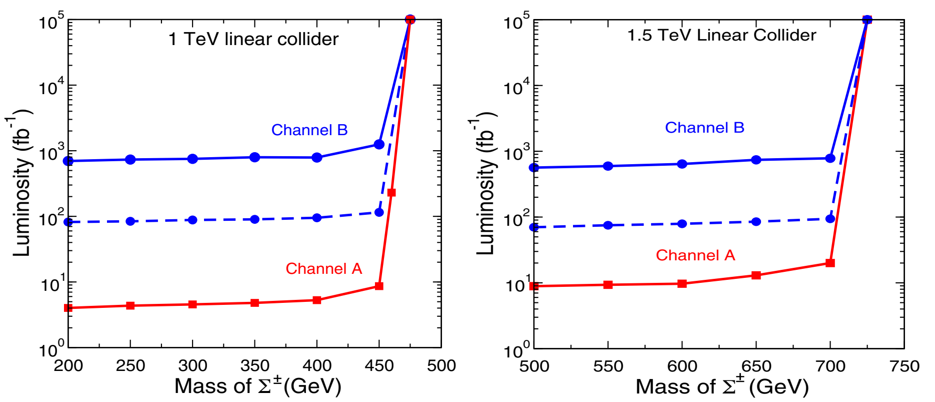

FIG. 11. The integrated luminosity for discovery (solid line) as a function of the mass of the singly charged fermion (M_Σ) is shown for channels A and B at 1 TeV (left) and 1.5 TeV (right) e^+e^- collider. The integrated luminosity for exclusion (dotted line) is also shown for channel B.

The requirement of exactly two leptons with opposite sign in channel B makes the cross section smaller than channel A. The largest background contribution comes from $t\bar{t}+$ jets due to the large cross section. We further check that the additional cuts on kinematic variables such as H_T, S_T, or MET would reduce the signal efficiency effectively; hence we did not impose them. Even though the signal cross section in channel B is less, we find that it is an excellent channel to reconstruct the invariant mass of M_Σ from the ℓjj distribution. We show the distribution for two cases, $M_\Sigma = 400$ and 600 GeV at $\sqrt{s} = 1$ and 1.5 TeV, respectively, in Fig. 10.

1. Result

For the study in the e^+e^- collider, the background is larger compared to the LHC scenario. Hence, Eq. (10) reduces to a simple form of $S/\sqrt{B}$. The integrated luminosity for discovery as a function of the mass of the singly charged fermion is shown in Fig. 11. We find that the discovery potential of channel A is much better than channel B, i.e., the required integrated luminosity is less in channel A for $M_\Sigma \leq 450$ and $M_\Sigma \leq 750$ GeV, at $\sqrt{s} = 1$ and 1.5 TeV, respectively. With $\lesssim 20$ fb^{-1} luminosity, it is possible to discover in the region of $M_\Sigma \leq 700$ GeV with 5σ significance in channel A, whereas the required luminosity for 5σ discovery is $\lesssim 1000$ fb^{-1} for the same in channel B. For 95% exclusion limit, the entire mass region can be probed with luminosity less than 100 fb^{-1} in channel B. The required luminosity in channel A is very small for the same, hence we do not plot them.

V. CONCLUSION AND OUTLOOK

We have discussed the discovery potential of the singly and the doubly charged fermions, which are components of

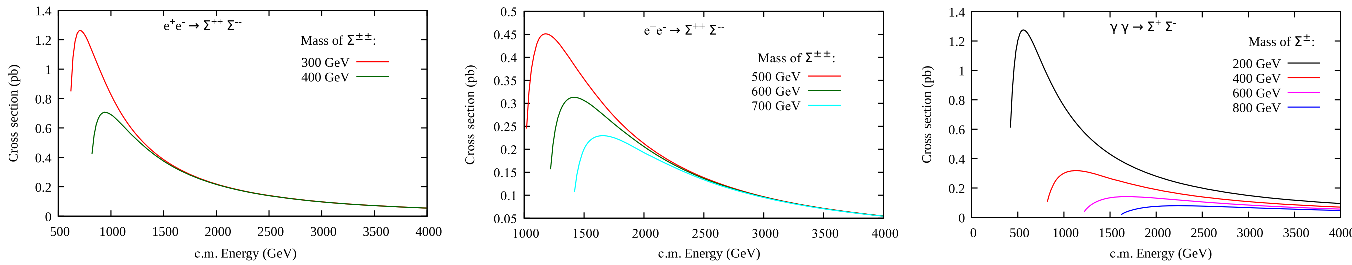

FIG. 12. Left and middle: the doubly charged quintuplet fermion production cross section as a function of the center of mass energy at the e^+e^- collider. Right: cross section for the singly charged quintuplet fermion production at the $\gamma\gamma$ collider.

a quintuplet, at the LHC and future e^+e^- colliders. Such a specific model, as we have considered, with quintuplet fermions and a scalar multiplet, predicts certain signatures that require alternate search strategies.

In the study of signatures at the LHC, we have discussed the possible multilepton and multi(lepton + jet) signatures of the doubly charged fermions, as they have larger cross sections compared to that of the singly charged fermions. For the doubly charged quintuplet fermion ($\Sigma^{\pm\pm}$), 5σ discovery might be possible at integrated luminosity of 3000 fb^{-1} at the 14 TeV LHC if $M_\Sigma \le 980$ GeV. The exclusion limit can be extended up to 1.2 TeV with the same parameters.

On the other hand, linear colliders, such as the e^+e^- collider, offer a much cleaner environment to study the signatures associated with multiple jets. Thus, the signals have the advantage of a larger cross section $\times$ BR, where the W/Z bosons decay into jets. We find that the singly charged fermion ($\Sigma^\pm$) shows a great discovery potential at the e^+e^- collider, unlike the case of the LHC. There might be a possibility of 5σ discovery with 1000 fb^{-1} luminosity at the e^+e^- collider for $M_\Sigma \le 700$ GeV. Similar kinds of final states also exist for the doubly charged quintuplet fermion but with more leptons and jets, making the analysis much more complicated. Thus, we will address it somewhere else. The cross sections for the pair production of the doubly charged fermions at the e^+e^- collider are shown in Fig. 12 (left and middle).

An e^+e^- linear collider can also be operated as a $\gamma\gamma$ and an $e^-\gamma$ collider, as illustrated in Refs. [70,71]. The highly intense photons for the collision are obtained by Compton backscattering laser photons on intense high-energy electron beams. Because of the coupling with photon, charged particles can be produced with a considerably high cross section at these photon colliders. In the present model, the production of the singly charged quintuplet fermions is possible via $\gamma\gamma \to \Sigma^+\Sigma^-$, $e^-\gamma \to \Sigma^+\phi--$, and $e^-\gamma \to \Sigma^-\phi^{0^*}$ modes, along with the conjugate process in each case. The production cross section for the singly charged quintuplet fermion at the $\gamma\gamma$ collider is shown in Fig. 12 (right) as a function of the center of mass energy. These production modes, alone or combined with e^+e^- collision, show a great potential at future linear colliders. Over all, the nonstandard decay modes of the quintuplet fermions offer different signals that require alternate search strategies and there might be an opportunity for discovery and/or exclusion at the HL-LHC and future linear colliders.

ACKNOWLEDGMENTS

N. K. acknowledges the support from the Dr. D. S. Kothari Postdoctoral scheme (201819-PH/18-19/0013). N. K. would also like to thank the IDT-WG3 Physics Potential Group of ILC for giving a chance to present this paper in their workshop. V. S. thanks Brajesh Choudhary for access to computers bought under the aegis of Grant No. SR-MF/PS-0212014-DUB (G) of the DST (India).

[1] Georges Aad *et al.*, Observation of a new particle in the search for the Standard Model Higgs boson with the ATLAS detector at the LHC, Phys. Lett. B **716**, 1 (2012).
[2] Serguei Chatrchyan *et al.*, Observation of a new boson at a mass of 125 GeV with the CMS experiment at the LHC, Phys. Lett. B **716**, 30 (2012).
[3] B. Abi *et al.*, Measurement of the Positive Muon Anomalous Magnetic Moment to 0.46 ppm, Phys. Rev. Lett. **126**, 141801 (2021).
[4] P. A. Zyla *et al.*, Review of particle physics, Prog. Theor. Exp. Phys. **2020**, 083C01 (2020).
[5] Rabindra N. Mohapatra and Goran Senjanovic, Neutrino Mass and Spontaneous Parity Nonconservation, Phys. Rev. Lett. **44**, 912 (1980).
[6] W. Konetschny and W. Kummer, Nonconservation of total lepton number with scalar bosons, Phys. Lett. **70B**, 433 (1977).
[7] M. Magg and C. Wetterich, Neutrino mass problem and gauge hierarchy, Phys. Lett. **94B**, 61 (1980).

[8] J. Schechter and J. W. F. Valle, Neutrino masses in $SU(2) \times U(1)$ theories, Phys. Rev. D **22**, 2227 (1980).
[9] T. P. Cheng and Ling-Fong Li, Neutrino masses, mixings and oscillations in $SU(2) \times U(1)$ models of electroweak interactions, Phys. Rev. D **22**, 2860 (1980).
[10] George Lazarides, Q. Shafi, and C. Wetterich, Proton lifetime and fermion masses in an SO(10) model, Nucl. Phys. **B181**, 287 (1981).
[11] Rabindra N. Mohapatra and Goran Senjanovic, Neutrino masses and mixings in gauge models with spontaneous parity violation, Phys. Rev. D **23**, 165 (1981).
[12] Robert Foot, H. Lew, X. G. He, and Girish C. Joshi, Seesaw neutrino masses induced by a triplet of leptons, Z. Phys. C **44**, 441 (1989).
[13] Yi Liao, Cascade Seesaw for tiny neutrino mass, J. High Energy Phys. 06 (2011) 098.
[14] K. S. Babu, S. Nandi, and Zurab Tavartkiladze, New mechanism for neutrino mass generation and triply charged Higgs bosons at the LHC, Phys. Rev. D **80**, 071702 (2009).
[15] Zurab Tavartkiladze, Naturally light neutrinos and unification in theories with low scale quantum gravity, Phys. Lett. B **528**, 97 (2002).
[16] Kresimir Kumericki, Ivica Picek, and Branimir Radovcic, TeV-scale seesaw with quintuplet fermions, Phys. Rev. D **86**, 013006 (2012).
[17] Rabindra N. Mohapatra and Jogesh C. Pati, Left-right gauge symmetry and an isoconjugate model of *CP* violation, Phys. Rev. D **11**, 566 (1975).
[18] G. Senjanovic and Rabindra N. Mohapatra, Exact left-right symmetry and spontaneous violation of parity, Phys. Rev. D **12**, 1502 (1975).
[19] Sanjib Kumar Agarwalla, Kirtiman Ghosh, and Ayon Patra, Sub-TeV quintuplet minimal dark matter with left-right symmetry, J. High Energy Phys. 05 (2018) 123.
[20] P. Ko and Takaaki Nomura, $SU(2)_L \times SU(2)_R$ minimal dark matter with 2 TeV W', Phys. Lett. B **753**, 612 (2016).
[21] Yi Cai, Xiao-Gang He, Michael Ramsey-Musolf, and Lu-Hsing Tsai, RνMDM and lepton flavor violation, J. High Energy Phys. 12 (2011) 054.
[22] Marco Cirelli and Alessandro Strumia, Minimal dark matter: Model and results, New J. Phys. **11**, 105005 (2009).
[23] Ian Low, Witold Skiba, and David Tucker-Smith, Little Higgs bosons from an antisymmetric condensate, Phys. Rev. D **66**, 072001 (2002).
[24] Nilanjana Kumar and Soumya Sadhukhan, Emergent 2HDM in the Low-Skiba-Smith little Higgs model: Musings from flavor and electroweak physics, Phys. Rev. D **103**, 055011 (2021).
[25] G. Pancheri and Y. N. Srivastava, Weak isospin spectroscopy of excited quarks and leptons, Phys. Lett. **146B**, 87 (1984).
[26] S. Biondini and O. Panella, Exotic leptons at future linear colliders, Phys. Rev. D **92**, 015023 (2015).
[27] R. Leonardi, O. Panella, and L. Fanò, Doubly charged heavy leptons at LHC via contact interactions, Phys. Rev. D **90**, 035001 (2014).
[28] E. Eichten, Kenneth D. Lane, and Michael E. Peskin, New Tests for Quark and Lepton Substructure, Phys. Rev. Lett. **50**, 811 (1983).
[29] N. Cabibbo, L. Maiani, and Y. Srivastava, Anomalous Z decays: Excited leptons?, Phys. Lett. **139B**, 459 (1984).
[30] Marco Cirelli, Nicolao Fornengo, and Alessandro Strumia, Minimal dark matter, Nucl. Phys. **B753**, 178 (2006).
[31] F. del Aguila, J. de Blas, and M. Perez-Victoria, Effects of new leptons in electroweak precision data, Phys. Rev. D **78**, 013010 (2008).
[32] Teng Ma, Bin Zhang, and Giacomo Cacciapaglia, Doubly charged lepton from an exotic doublet at the LHC, Phys. Rev. D **89**, 093022 (2014).
[33] Nabarun Chakrabarty, Doubly charged scalars and vector-like leptons confronting the muon $g-2$ anomaly and Higgs vacuum stability, Eur. Phys. J. Plus **136**, 1183 (2021).
[34] Francisco del Aguila, Adrian Carmona, and Jose Santiago, Tau custodian searches at the LHC, Phys. Lett. B **695**, 449 (2011).
[35] Jin-Wei Wang, Xiao-Jun Bi, Qian-Fei Xiang, Peng-Fei Yin, and Zhao-Huan Yu, Exploring triplet-quadruplet fermionic dark matter at the LHC and future colliders, Phys. Rev. D **97**, 035021 (2018).
[36] Takaaki Nomura and Hiroshi Okada, Neutrino mass with large $SU(2)_L$ multiplet fields, Phys. Rev. D **96**, 095017 (2017).
[37] Nilanjana Kumar, Takaaki Nomura, and Hiroshi Okada, Scotogenic neutrino mass with large $SU(2)_L$ multiplet fields, Eur. Phys. J. C **80**, 801 (2020).
[38] You Yu, Chong-Xing Yue, and Shuo Yang, Signatures of the quintuplet leptons at the LHC, Phys. Rev. D **91**, 093003 (2015).
[39] Chian-Shu Chen and Ya-Juan Zheng, LHC signatures for the cascade seesaw mechanism, Prog. Theor. Exp. Phys. **2015**, 103B02 (2015).
[40] A. Ozansoy, Doubly charged lepton search potential of the FCC-based energy-frontier electron-proton colliders, Adv. High Energy Phys. **2020**, 9234130 (2020).
[41] Yu-Chen Guo, Chong-Xing Yue, and Zhi-Cheng Liu, The signatures of doubly charged leptons in future linear colliders, J. Phys. G **44**, 085004 (2017).
[42] H. Abramowicz *et al.*, Physics at the CLIC $e^+ e^-$ Linear Collider—Input to the Snowmass process 2013, in Proceedings of the 2013 Community Summer Study on the Future of US Particle Physics: Snowmass on the Mississippi (CSS2013) : Minneapolis, MN, USA, 2013, http://cds.cern.ch/record/1563377.
[43] Strahinja Lukić, Physics highlights at ILC and CLIC, in *Proceedings of the 12th International School-Seminar on the Actual Problems of Microworld Physics: Gomel, Belarus* (2013), Vol. 1, pp. 39–53, http://cds.cern.ch/record/1621591.
[44] Qing-Guo Zeng, Production of the quintuplet leptons in future high energy linear $e^+ e^-$ colliders, Nucl. Phys. **B905**, 251 (2016).
[45] Salvatore Rappoccio, The experimental status of direct searches for exotic physics beyond the Standard Model at the Large Hadron Collider, Rev. Phys. **4**, 100027 (2019).
[46] A. Buckley, J. M. Butterworth, L. Corpe, D. Huang, and P. Sun, New sensitivity of current LHC measurements to vector-like quarks, SciPost Phys. **9**, 069 (2020).

[47] Albert M. Sirunyan *et al.*, Search for vector-like leptons in multilepton final states in proton-proton collisions at $\sqrt{s} = 13$ TeV, Phys. Rev. D **100**, 052003 (2019).

[48] G. Abbiendi *et al.*, Search for charged Higgs bosons: Combined results using LEP data, Eur. Phys. J. C **73**, 2463 (2013).

[49] Albert M. Sirunyan *et al.*, Search for charged Higgs bosons in the $H^{\pm} \to \tau^{\pm}\nu_{\tau}$ decay channel in proton-proton collisions at $\sqrt{s} = 13$ TeV, J. High Energy Phys. 07 (2019) 142.

[50] Morad Aaboud *et al.*, Search for doubly charged Higgs boson production in multi-lepton final states with the ATLAS detector using proton–proton collisions at $\sqrt{s} = 13$ TeV, Eur. Phys. J. C **78**, 199 (2018).

[51] Georges Aad *et al.*, Search for doubly and singly charged Higgs bosons decaying into vector bosons in multi-lepton final states with the ATLAS detector using proton-proton collisions at $\sqrt{s} = 13$ TeV. J. High Energy Phys. 06 (2021) 146.

[52] Morad Aaboud *et al.*, Search for doubly charged scalar bosons decaying into same-sign W boson pairs with the ATLAS detector, Eur. Phys. J. C **79**, 58 (2019).

[53] Richard D. Ball *et al.*, Parton distributions for the LHC run II, J. High Energy Phys. 04 (2015) 040.

[54] Richard D. Ball, Valerio Bertone, Stefano Carrazza, Luigi Del Debbio, Stefano Forte, Alberto Guffanti, Nathan P. Hartland, and Juan Rojo, Parton distributions with QED corrections, Nucl. Phys. **B877**, 290 (2013).

[55] A. D. Martin, R. G. Roberts, W. J. Stirling, and R. S. Thorne, Parton distributions incorporating QED contributions, Eur. Phys. J. C **39**, 155 (2005).

[56] Carl Schmidt, Jon Pumplin, Daniel Stump, and C. P. Yuan, CT14QED parton distribution functions from isolated photon production in deep inelastic scattering, Phys. Rev. D **93**, 114015 (2016).

[57] Adam Alloul, Neil D. Christensen, Céline Degrande, Claude Duhr, and Benjamin Fuks, FeynRules 2.0—A complete toolbox for tree-level phenomenology, Comput. Phys. Commun. **185**, 2250 (2014).

[58] Neil D. Christensen and Claude Duhr, FeynRules—Feynman rules made easy, Comput. Phys. Commun. **180**, 1614 (2009).

[59] J. Alwall, R. Frederix, S. Frixione, V. Hirschi, F. Maltoni, O. Mattelaer, H. S. Shao, T. Stelzer, P. Torrielli, and M. Zaro, The automated computation of tree-level and next-to-leading order differential cross sections, and their matching to parton shower simulations, J. High Energy Phys. 07 (2014) 079.

[60] Richard D. Ball *et al.*, Parton distributions with LHC data, Nucl. Phys. **B867**, 244 (2013).

[61] Debajyoti Choudhury, Kuldeep Deka, and Nilanjana Kumar, Looking for a vectorlike B quark at the LHC using jet substructure, Phys. Rev. D **104**, 035004 (2021).

[62] Glen Cowan, Kyle Cranmer, Eilam Gross, and Ofer Vitells, Asymptotic formulae for likelihood-based tests of new physics, Eur. Phys. J. C **71**, 1554 (2011); **73**, 2501(E) (2013).

[63] T. P. Li and Y. Q. Ma, Analysis methods for results in gamma-ray astronomy, Astrophys. J. **272**, 317 (1983).

[64] Robert D. Cousins, James T. Linnemann, and Jordan Tucker, Evaluation of three methods for calculating statistical significance when incorporating a systematic uncertainty into a test of the background-only hypothesis for a Poisson process, Nucl. Instrum. Methods Phys. Res., Sect. A **595**, 480 (2008).

[65] Liangliang Shang, Mengmeng Wang, Zhaoxia Heng, and Bingfang Yang, Search for the singlet vector-like lepton at future $e^{+}e^{-}$ colliders, Eur. Phys. J. C **81**, 415 (2021).

[66] Arindam Das, Sanjoy Mandal, and Tanmoy Modak, Testing triplet fermions at the electron-positron and electron-proton colliders using fat jet signatures, Phys. Rev. D **102**, 033001 (2020).

[67] Arindam Das and Sanjoy Mandal, Bounds on the triplet fermions in type-III seesaw and implications for collider searches, Nucl. Phys. **B966**, 115374 (2021).

[68] G. Azuelos and A. Djouadi, New fermions at $e^{+}e^{-}$ colliders. II. Signals and backgrounds, Z. Phys. C **63**, 327 (1994).

[69] Halina Abramowicz *et al.*, The International Linear Collider Technical Design Report—Volume 4: Detectors, Reports No. ILC-REPORT-2013-040, ANL-HEP-TR- 13-20, BNL-100603-2013-IR, IRFU-13-59, CERN-ATS-2013-037, COCKCROFT- 13-10, CLNS-13-2085, DESY-13-062, FERMILAB-TM-2554, IHEP-AC-ILC-2013- 001, INFN-13-04-LNF, JAI-2013-001, JINR-E9-2013-35, JLAB-R-2013-01, KEK- REPORT-2013-1, KNU-CHEP-ILC-2013-1, LLNL-TR-635539, SLAC-R-1004, ILC- HIGRADE-REPORT-2013-003, 2013.

[70] K. J. Kim and A. Sessler, Gamma-gamma colliders, Reports No. LBL-39093, LBNL-39093, CBP-NOTE-185, 1996, https://www.osti.gov/biblio/378863.

[71] Albert De Roeck, Physics at a $\gamma\gamma$, $e\gamma$ and $e^{-}e^{-}$ option for a linear collider, in *Proceedings of the 4th ECFA/DESY Workshop on Physics and Detectors for a 90-GeV to 800-GeV Linear e+ e- Collider* (2003), pp. 69–78, http://cds.cern.ch/record/682646.